Unraveling the $\tilde{A}^1B_1 \leftarrow \tilde{X}^1A_1$ Spectrum of CCl_2: The Renner−Teller Effect, Barrier to Linearity, and Vibrational Analysis Using an Effective Polyad Hamiltonian

Craig Richmond,[†] Chong Tao,[‡] Calvin Mukarakate,[‡] Haiyan Fan,[‡] Klaas Nauta,[†] Timothy W. Schmidt,[†] Scott H. Kable,*[,†] and Scott A. Reid*[,‡]

School of Chemistry, University of Sydney, Sydney, NSW 2006, Australia, and Department of Chemistry, Marquette University, Milwaukee, Wisconsin 53201-1881

Received: August 4, 2008; Revised Manuscript Received: September 11, 2008

We report studies aimed at unraveling the complicated structure of the CCl_2 $\tilde{A}^1B_1 \leftarrow \tilde{X}^1A_1$ system. We have remeasured the fluorescence excitation spectrum from ~17 500 to 24 000 cm^{-1} and report the term energies and *A* rotational constants of many new bands for both major isotopologues ($C^{35}Cl_2$, $C^{35}Cl^{37}Cl$). We fit the observed term energies to a polyad effective Hamiltonian model and demonstrate that a single resonance term accounts for much of the observed mixing, which begins ~1300 cm^{-1} above the vibrationless level of the $\tilde{A}^1B_1$ state. The derived $\tilde{A}^1B_1$ vibrational parameters are in excellent agreement with ab initio predictions, and the mixing coefficients deduced from the polyad model fit are in close agreement with those derived from direct fits of single vibronic level (SVL) emission intensities. The approach to linearity and thus the Renner−Teller (RT) intersection is probed through the energy dependence of the *A* rotational constant and fluorescence lifetime measurements, which indicate a barrier height above the vibrationless level of the $\tilde{X}^1A_1$ state of ~23 000−23 500 cm^{-1}, in excellent agreement with ab initio theory.

I. Introduction

Carbenes are an important class of reactive intermediates.[1−6] Their divalent carbon atom gives rise to singlet and triplet configurations of similar energy but very different reactivity, and, over the past decade, significant experimental progress has been made in determining the singlet−triplet splitting for a number of simple carbenes.[7−23] For triatomic carbenes such as CCl_2 which have singlet ground states, the ground-state electronic configuration consists of the two nonbonding electrons paired in an in-plane sp^2-hybridized orbital centered on the carbon atom, giving rise to a strongly bent equilibrium structure. Promotion of one electron to an out-of-plane carbon-centered p_x orbital gives rise to singlet and triplet excited states with a marked increase in bond angle. The ground ($\tilde{X}$) and excited ($\tilde{A}$) singlet states form a Renner−Teller pair in the linear configuration, and, considering the low-lying triplet state, the spectroscopy of the $\tilde{X} \rightarrow \tilde{A}$ system is complicated by a mix of Renner−Teller (RT) and spin−orbit interactions. Additionally, in systems such as CFCl[24] and CFBr[25] where the RT intersection occurs above thermochemical thresholds for dissociation, predissociation is a further complication. In order to understand the complicated spectroscopy associated with these simple carbenes, we and others have embarked on studies of the $\tilde{X} \rightarrow \tilde{A}$ transitions in singlet carbenes such as CHF where the RT intersection lies below thermochemical thresholds for dissociation. For example, we showed that the lifetimes of CHF $\tilde{A}$ state levels with $K'_a \geq 1$ display a textbook example of lifetime lengthening with increasing energy, due to the RT interaction.[26] The approach to linearity in the $\tilde{A}$ state is evidenced in a sharp increase in the *A* rotational constant with bending excitation,[27,28] and a minimum in the vibrational intervals near seven quanta of bending vibration. The derived barrier height is consistent with ab initio predictions.[29] Singlet−triplet perturbations in the $\tilde{A}$ state of CHF were characterized by polarization quantum beat spectroscopy.[30−32]

Dichloromethylene (CCl_2) is one of the best studied, but possibly least understood, of all the triatomic halocarbenes.[7−9,22,33−79] As discussed recently,[41] the fluorescence excitation spectrum of the $\tilde{A}^1B_1 \leftarrow \tilde{X}^1A_1$ system of CCl_2 can be separated into three distinct regions. Region 1, which lies below 20 300 cm^{-1} and has been studied extensively,[33−45] most completely by Clouthier and Karolczak,[42,43] displays regular vibrational structure, and a Dunham expansion fit of the band origins for the $C^{35}Cl_2$ and $C^{35}Cl^{37}Cl$ isotopologues well reproduces the experimental term energies. In Region 2, lying between 20 300 cm^{-1} and roughly 22 500 cm^{-1}, the rotational structure of the bands is largely unperturbed; however, vibrational assignments have not been made due to extensive vibrational mixing, presumed to arise from near resonances among the states 1^n2^m having the same polyad number $p = 2n + m$.[41] Above ~22 500 cm^{-1} (Region 3), the rotational structure of all bands changes markedly, such that above ~23 000 cm^{-1} only subbands terminating in $K'_a = 0$ appear strongly in the spectra, suggesting (by analogy to CHF) that the RT intersection has been exceeded.[41]

In this work, we set out to unravel the complicated structure of the CCl_2 $\tilde{A}^1B_1 \leftarrow \tilde{X}^1A_1$ system. We have remeasured the spectrum from ~17 500 to 24 000 cm^{-1}, or from polyad $p = 1$ to $p = 21$, and report the term energy and *A* rotational constant for many new bands of both major isotopologues ($C^{35}Cl_2$, $C^{35}Cl^{37}Cl$). We fit the observed term energies to a polyad effective Hamiltonian model and demonstrate that a single resonance term accounts for much of the observed mixing. Vibrational parameters derived from this fit are compared with the predictions of high-level ab initio theory, and the mixing coefficients deduced from the polyad model fit are compared with those derived from direct fits of single vibronic level (SVL)

* Corresponding authors. E-mail: scott.reid@mu.edu; s.kable@chem.usyd.edu.au.
[†] University of Sydney.
[‡] Marquette University.

10.1021/jp806944q CCC: $40.75
Published on Web 10/17/2008

emission intensities. We examined the approach to linearity and the RT intersection through the energy dependence of the *A* rotational constant and fluorescence lifetime measurements, and our estimated barrier height is compared with the predictions of ab initio theory.

II. Experimental Section

The experiments were carried out at Marquette University (fluorescence excitation spectroscopy and lifetime measurements) and the University of Sydney (fluorescence excitation spectroscopy and SVL fluorescence). The relevant techniques have already been discussed in detail,[20−22,26,27,29−32,41] and so only an overview is presented here.

Marquette. CCl_2 was produced using a pulsed electrical discharge through a ∼1−2% mixture of CCl_4 (Aldrich) seeded in high-purity He. The precursor was kept in a stainless steel bubbler through which pure He gas was passed at a pressure of 3 bar. The discharge was initiated by a +1 kV pulse of ∼100 μs duration, through a current-limiting 10 kΩ ballast resistor. The timing of laser, nozzle, and discharge firing was controlled by a digital delay generator, which also generated a variable width gate pulse for the high-voltage pulser. A Nd:YAG-pumped dye laser (0.15 cm^{-1} line width) intersected the free jet expansion about 1 cm (13 nozzle diameters) downstream. The laser beam was not focused, and typical pulse energies were ∼1−2 mJ in a ∼3 mm diameter beam. CCl_2 fluorescence was collimated, mutually orthogonal to the jet and laser axes, by a 2 in. diameter f/2.4 lens, and then focused through a long-pass filter onto a photomultiplier using a 2 in. diameter f/3.0 lens. A small portion of the laser beam was directed into a Fe:Ne or Fe:Ar hollow cathode lamp for absolute frequency calibration using the optogalvanic effect. All frequencies in this work were calibrated to air wavelengths.

For fluorescence lifetime measurements, the orientation of the nozzle was flipped so that, while remaining perpendicular to the laser beam, it faced the collection optics. This geometry minimized flyout effects, and past experience in our laboratory has shown that fluorescence lifetimes exceeding 10 μs can be accurately measured in this way. Typically, 2500 fluorescence waveforms were averaged using a 1 GHz digital storage oscilloscope, and repeated five times. Lifetimes were obtained by fitting each waveform to a single-exponential function, and the average of the five measurements reported.

Sydney. CCl_2 was produced by pyrolysis of 1% $CHCl_3$ in He (40 bar) in an oven attached to the orifice of the pulsed nozzle. CCl_2 molecules were probed by an excimer-pumped dye laser with similar laser and detection specifications and configuration as the Marquette experiments. Fluorescence was imaged into a small monochromator (20 nm bandpass) for LIF experiments. For SVL fluorescence experiments, the emission was imaged onto the slits of a 0.75 m scanning spectrometer. In each case, fluorescence was detected by a PMT, processed using a boxcar integrator, and collected on a computer for further processing. Laser wavelength was calibrated using a wavemeter.

III. Results and Discussion

A. Excitation Spectrum and $\tilde{A}$ State Energies. The $\tilde{A}^1B_1 \leftarrow \tilde{X}^1A_1$ fluorescence excitation spectra from 18 000 to 24 000 cm^{-1}, measured in the Marquette and Sydney laboratories, are essentially identical, with only a minor difference in rotational temperature, which was typically 10−20 K. An example experimental (Marquette) and simulated spectrum for the $p = 7$ polyad is shown in Figure 1. The simulated

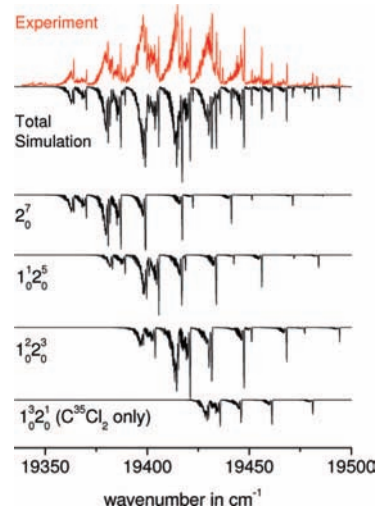

Figure 1. Experimental (upper) and simulated spectrum of the $p = 7$ polyad in the $\tilde{A}^1B_1 \leftarrow \tilde{X}^1A_1$ system of CCl_2. The composite simulation and the individual simulations for each band are shown. Except where noted, each simulation includes both major isotopomers ($C^{35}Cl_2$, $C^{35}Cl^{37}Cl$), which were scaled in a 9:6 ratio based upon the expected isotopic abundances.

spectrum includes the two dominant isotopologues ($C^{35}Cl_2$ and $C^{35}Cl^{37}Cl$) for each band and was obtained by fitting the positions of the sharp ^rR_K bandheads, with the *B* and *C* constants fixed at the value for the $\tilde{A}^1B_1$ origin. In this way the term energies and *A* rotational constants were determined for each band. Experimental and simulated spectra of all polyads measured in this work are provided in the Supporting Information.

We performed a fit of the observed term energies up to 23 600 cm^{-1} for the $C^{35}Cl_2$ and $C^{35}Cl^{37}Cl$ isotopologues using two different models. Model 1 was the traditional anharmonic (Dunham expansion) model, here given by[80]

$$G^0(v_1, v_2) = T_{00} + v_1\omega_1^0 + v_2\omega_2^0 + v_1^2x_{11}^0 + v_1v_2x_{12}^0 + v_2^2x_{22}^0 \quad (1)$$

where G^0 is the vibrational term energy (cm^{-1}), T_{00} is the electronic term energy, v_i are the number of quanta of modes 1 (stretch) and 2 (bend), ω_i are the harmonic energies, and x_{ij} are the anharmonicity constants. Previous studies have shown that the vibrational term energies up to 20 300 cm^{-1} are well fit to this model.[42,43]

Model 2 was an effective polyad Hamiltonian model, where the Dunham expansion terms formed the diagonal elements in the Hamiltonian matrix, and the off-diagonal elements incorporated a Fermi-resonance term of the form:

$$\langle v_1, v_2|H_F|v_1 - 1, v_2 + 2\rangle = k_{122}[(v_1)(v_2 + 1)(v_2 + 2)/8]^{1/2} \quad (2)$$

where H_F is the Fermi resonance coupling matrix element, and k_{122} represents the matrix element for the v_1:$2v_2$ Fermi resonance. In the harmonic oscillator limit, the matrix elements for coupling of higher Fermi polyads is given by the expression on the right-hand side of eq 2.

Table 1 displays the assignments, term energies, and deviations for both models. Overall, Model 2 provided a much improved representation of the data up to 23 600 cm^{-1}, with the standard deviation for the $C^{35}Cl_2$ data set of 54 levels decreasing from 7.0 cm^{-1} (Model 1) to 1.2 cm^{-1} (Model 2),

TABLE 1: Band Origins, Assignments, Fit Deviations, and *A* Rotational Constants for the CCl_2 Bands Measured in This Work

$C^{35}Cl_2$ assignment	$C^{35}Cl_2$ origin (cm^{-1})[a]	Model 1 obsd − calcd (cm^{-1})[b]	Model 2 obsd − calcd (cm^{-1})	$C^{35}Cl^{37}Cl$ assignment	$C^{35}Cl^{37}Cl$ origin (cm^{-1})[a]	Model 1 obsd − calcd (cm^{-1})	Model 2 obsd − calcd (cm^{-1})	*A* (cm^{-1})[c]
2_0^1	17559.5	6.2	0.1	2_0^1	17556.0	2.3	−0.7	3.74
2_0^2	17861.7	3.8	−0.6	2_0^2	17855.4	1.7	−1.2	3.82
2_0^3	18165.2	2.2	0.2	2_0^3	18156.0	1.7	−0.4	3.96
$1_0^1 2_0^1$	18188.7	1.8	0.8	$1_0^1 2_0^1$	18181.8	1.5	1.5	3.84
2_0^4	18468.3	−0.3	0.3	2_0^4	18456.4	0.8	−0.2	4.11
$1_0^1 2_0^2$	18489.4	0.7	0.2	$1_0^1 2_0^2$	18479.2	1.3	0.7	3.95
2_0^5	18771.6	−3.0	0.7	2_0^5	18757.0	−0.4	0.2	4.30
$1_0^1 2_0^3$	18790.5	−0.5	−0.1	$1_0^1 2_0^3$	18777.5	1.5	0.5	4.09
$1_0^2 2_0^1$	18809.8	−1.1	0.7	–	–	–	–	3.96
2_0^6	19074.3	−6.8	0.6	2_0^6	19057.5	−2.4	0.6	4.49
$1_0^1 2_0^4$	19092.1	−1.6	−0.1	$1_0^1 2_0^4$	19076.0	1.2	0.3	4.23
$1_0^2 2_0^2$	19109.3	−0.6	0.2	$1_0^2 2_0^2$	19095.4	0.6	1.5	4.06
2_0^7	19376.7	−11.4	0.5	2_0^7	19357.7	−5.2	0.7	4.59
$1_0^1 2_0^5$	19393.4	−3.5	−0.3	$1_0^1 2_0^5$	19374.8	0.7	0.2	4.40
$1_0^2 2_0^3$	19408.9	−0.5	−0.5	$1_0^2 2_0^3$	19391.8	1.3	0.6	4.19
$1_0^3 2_0^1$	19423.7	−1.6	0.5	–	–	–	–	4.06
2_0^8	19694.5	−6.1	−0.5	$1_0^1 2_0^6$	19673.4	−0.7	0.0	4.65
$1_0^1 2_0^6$	19709.2	−0.1	−0.7	$1_0^2 2_0^4$	19688.6	1.8	−0.1	4.34
$1_0^3 2_0^2$	19721.9	0.4	−0.6	$1_0^3 2_0^2$	19702.7	−1.9	−0.2	4.20
1_0^4	19733.1	−4.1	0.9	–	–	–	–	3.87
$1_0^1 2_0^7 - 1_0^3 2_0^3$	20009.4	−0.3	−0.7	$1_0^1 2_0^7 - 1_0^3 2_0^3$	19985.9	2.2	−0.5	4.53
$1_0^2 2_0^5 - 1_0^4 2_0^1$	20021.5	3.4	−0.6	$1_0^2 2_0^5 + 1_0^3 2_0^3$	19999.2	1.4	−0.1	4.28
$1_0^4 2_0^1 + 1_0^3 2_0^3$	20031.5	1.4	0.4	–	–	–	–	4.14
–	–	–	–	$1_0^1 2_0^8 - 1_0^3 2_0^4$	20283.4	2.2	−0.6	4.90
$1_0^1 2_0^8 - 1_0^4 2_0^2$	20320.2	5.0	−1.2	$1_0^2 2_0^6 - 1_0^4 2_0^2$	20295.1	3.5	−1.0	4.49
$1_0^4 2_0^2$	20328.1	4.7	−1.8	$1_0^3 2_0^4 + 1_0^4 2_0^2$	20305.5	−1.7	−0.7	4.31
$1_0^5 + 1_0^4 2_0^2$	20334.4	−0.8	−0.2	–	–	–	–	4.19
$-1_0^3 2_0^5 - 2_0^{11}$	20591.6	−21.2	−3.3	$1_0^3 2_0^5 + 2_0^{11}$	20563.8	−15.6	−3.7	4.70
$-1_0^5 2_0^1$	20629.0	8.2	0.1	$-1_0^5 2_0^1$	20600.8	2.9	−1.6	4.48
$1_0^3 2_0^5 + 1_0^2 2_0^7$	20637.1	11.9	−0.5	$1_0^5 2_0^1 + 1_0^4 2_0^3$	20609.4	−5.5	0.2	4.28
$-1_0^4 2_0^4$	20895.2	−16.4	2.4	$-1_0^3 2_0^5 - 2_0^{12}$	20865.6	−14.6	1.7	4.61
1_0^6	20922.7	2.5	−1.2	–	–	–	–	4.50
$1_0^1 2_0^8$	20941.5	11.3	−1.0	$1_0^3 2_0^5$	20908.2	−12.7	−0.5	4.47
$-1_0^4 2_0^5$	21236.6	10.3	2.1	$1_0^6 2_0^1$	21192.0	1.2	−1.0	4.81
$1_0^2 2_0^9 + 1_0^1 2_0^{11}$	21247.5	7.5	−1.1	$1_0^3 2_0^7 + 1_0^2 2_0^9$	21208.6	3.1	−1.2	4.70
$1_0^5 2_0^4$	21483.8	−14.7	0.0	–	–	–	–	4.88
$-1_0^3 2_0^8 + 2_0^{14}$	21541.1	8.2	2.2	$-1_0^4 2_0^6$	21502.2	0.6	1.9	5.00
$1_0^2 2_0^{10} + 1_0^1 2_0^{12}$	21554.5	4.2	−1.1	$1_0^2 2_0^{10} + 1_0^1 2_0^{12}$	21510.8	4.0	−1.8	4.90
$-1_0^3 2_0^9 + 2_0^{15}$	21846.0	6.1	2.1	$-1_0^4 2_0^7 + 2_0^{15}$	21803.6	12.4	2.4	5.27
$1_0^6 2_0^3$	21862.5	1.4	−0.7	$1_0^2 2_0^{11} + 1_0^1 2_0^{13}$	21815.0	5.4	−1.3	5.15
$1_0^7 2_0^2 - 1_0^6 2_0^4$	22067.9	−3.7	0.2	–	–	–	–	5.20
–	–	–	–	-1_0^8	22058.8	−8.7	0.0	5.04
$-1_0^3 2_0^{10} + 2_0^{16}$	22152.2	4.8	2.6	$-1_0^3 2_0^{10} + 2_0^{16}$	22105.2	9.1	2.0	5.06
$1_0^1 2_0^{14} + 2_0^{16}$	22171.2	−1.2	−0.3	$1_0^2 2_0^{12} + 1_0^1 2_0^{14}$	22119.9	1.7	−1.1	5.35
$-1_0^5 2_0^7 - 2_0^{17}$	22434.5	4.3	1.1	$-1_0^5 2_0^7 - 1_0^4 2_0^9$	22389.5	8.4	1.9	5.90
$-1_0^3 2_0^{11} + 2_0^{17}$	22457.1	1.7	1.3	$-1_0^3 2_0^{11} + 2_0^{17}$	22407.6	5.9	1.8	5.90
$1_0^1 2_0^{15} + 2_0^{17}$	22480.4	−3.8	0.1	$1_0^1 2_0^{15} + 2_0^{17}$	22425.8	−1.6	−0.4	5.70
$-1_0^4 2_0^{10}$	22737.6	2.7	0.0	$-1_0^4 2_0^{10}$	22689.4	5.9	1.2	6.50
$-1_0^3 2_0^{12} + 2_0^{18}$	22763.4	−0.5	0.8	$-1_0^3 2_0^{12} + 2_0^{18}$	22710.2	2.4	1.2	6.20
$1_0^1 2_0^{16} + 2_0^{18}$	22790.2	−6.3	0.5	–	–	–	–	6.00
$1_0^8 2_0^3$	22955.8	11.5	0.6	–	–	–	–	7.65
$-1_0^4 2_0^{11}$	23040.8	0.7	−1.4	$-1_0^4 2_0^{11}$	22989.2	2.7	−0.2	9.7[d]
$-1_0^3 2_0^{13} + 2_0^{19}$	23069.8	−3.1	0.0	$-1_0^3 2_0^{13} + 2_0^{19}$	23013.3	−1.2	0.5	6.75
$-1_0^4 2_0^{12} + 1_0^1 2_0^{18}$	23344.5	−1.2	−2.8	$-1_0^4 2_0^{12} + 1_0^1 2_0^{18}$	23289.8	−1.0	−1.2	10.4[d]
$-1_0^2 2_0^{16} + 2_0^{20}$	23376.9	−5.4	−0.6	$-1_0^2 2_0^{16} + 2_0^{20}$	23317.0	−4.9	0.0	16.0[d]
–	–	–	–	$-1_0^4 2_0^{13} + 1_0^1 2_0^{19}$	23590.1	−4.4	−3.1	8.3[d]
$-1_0^2 2_0^{17} + 2_0^{21}$	23685.6	−6.6	−0.1	$1_0^3 2_0^{15} - 2_0^{21}$	23622.6	−7.2	0.8	13.1[d]
fit SD		**7.0**	**1.2**			**5.8**	**1.4**	

[a] Estimated uncertainty of ±0.1 cm^{-1}. [b] Observed − calculated. [c] Estimated uncertainty of ±0.02 cm^{-1}, except where noted. [d] Estimated uncertainty of ±0.1 cm^{-1}.

and that for the $C^{35}Cl^{37}Cl$ set of 46 levels from 5.8 cm^{-1} (Model 1) to 1.4 cm^{-1} (Model 2). One caveat should be made regarding the "assignments" in Table 1 for bands above ~20 000 cm^{-1}. We initially made zeroth-order assignments for these bands based upon the largest mixing coefficient for a given state; however, this has the disadvantage that the same assignment is sometimes given to more than one state. Thus, the assignments in Table 1 reflect the dominant zeroth-order states, i.e., all which have an absolute mixing coefficient ≥0.5. Levels with a negative sign indicate that the derived mixing coefficient was negative. These "assignments" should be considered only as labels, as all levels in a given polyad for polyads above 20 000 cm^{-1} are strongly mixed. Importantly, our analysis shows that this mixing can be adequately described with the single Fermi-resonance term, $k_{122} = -4.2$ cm^{-1}.

The mixing among levels within a given polyad are readily shown in the coefficients c_{ij}, defining the eigenfunctions in terms of the zeroth-order states, i.e.

$$|\psi_i\rangle = \sum_j c_{ij}\phi_j \quad \phi_j = |v_1, v_2\rangle \tag{3}$$

where $|v_1,v_2\rangle$ are the zeroth-order states and the sum runs over all levels *j* in a given polyad. Our analysis shows that the 18 800

TABLE 2: Vibrational Parameters for $CCl_2(\tilde{A})$: Experiment and Theory

	T_{00}[b]	ω_1^0	ω_2^0	x_{11}^0	x_{22}^0	x_{12}^0	k_{122}
			$C^{35}Cl_2$				
experiment							
Model 1[a]	17249.2(6)	641.2(3)	303.9(2)	−4.80(3)	0.23(1)	−2.81(3)	−
Model 2[a]	17256.9(6)	633.7(4)	302.3(2)	−3.81(5)	0.20(1)	−1.95(5)	−4.19(5)
ref 43	17255.672(15)	634.280(78)	302.618(22)	−2.638(68)	0.113(5)	−1.989(28)	−
theory							
ref 68	16989	633.7	304.0	−	−	−	−
			$C^{35}Cl^{37}Cl$				
experiment							
Model 1[a]	17254.3(7)	632.7(3)	299.1(2)	−3.59(3)	0.31(1)	−2.47(3)	−
Model 2[a]	17257.1(7)	628.7(4)	299.3(2)	−3.52(4)	0.19(1)	−1.92(6)	−3.73(7)
ref 43	17255.450(24)	631.54(26)	299.594(25)	−3.56(29)	0.140(5)	−1.987(95)	−

[a] This work. [b] One standard error in parentheses.

cm^{-1} polyad ($p = 5$), comprising the zero-order states $1_0^2 2_0^1$, $1_0^1 2_0^3$, and 2_0^5, is the highest energy polyad for which the squared diagonal coefficients (c_{ii}^2) are all greater than 0.8. At higher energies the mixing increases, so that even an approximate description of the observed states in terms of a zeroth-order picture is not valid. For example, in the 20 600 cm^{-1} polyad ($p = 11$), the largest of any squared coefficient, c_{ij}^2, is 0.42. A detailed listing of the wave functions predicted from our polyad analysis for both $C^{35}Cl_2$ and $C^{35}Cl^{37}Cl$ is provided in the Supporting Information.

B. Spectroscopic Constants. The vibrational parameters determined from the fits to Models 1 and 2 are compared in Table 2 with previous experiment and theory. Note that the parameters derived in ref 43 were obtained from a fit using Model 1 of the term energies up to 20 300 cm^{-1}. Despite some differences in assignments (Table 1), our derived vibrational parameters are consistent with the previous work. Converting the fit frequencies to harmonic frequencies using the relationship[80]

$$\omega_i = \omega_i^0 - x_{ii}^0 - \sum_{j \neq i} \frac{x_{ij}^0}{2} \tag{4}$$

we obtain (in cm^{-1}): $\omega_1 = 637.6(3)$, $\omega_2 = 304.3(2)$, in excellent agreement with the ab initio (CASPT2/cc-pVTZ) calculations of Sendt and Bacskay,[68] which gave (in cm^{-1}): $\omega_1 = 633.7$, $\omega_2 = 304.0$.

C. Single Vibronic Level Fluorescence Spectra and $\tilde{A}$ State Wave functions. Figure 2a−c contains examples of experimental and simulated SVL emission spectra. Panel (a) displays a level from $p = 4$, and panels (b) and (c) display different levels from $p = 8$. Polyad $p = 4$ is at energies below the onset on significant mixing (all $c_{ii}^2 > 0.9$), and $p = 8$ has highly variable values for c_{ij}^2, with frequency analysis indicating the levels to be significantly mixed.

Within each panel, the top spectrum is an experimental SVL emission spectrum, and the inverted spectra are simulations. The bottom simulations in each panel are based on emission from unmixed excited states (where Model 1 would be appropriate), as performed previously.[41] The zeroth-order excited states used for the simulations are shown beside the upper left corner of each panel. The simulation for $p = 4$ is quite a good fit, which is not unexpected for a state with very little mixing. In contrast, the fit to levels in $p = 8$ is quite poor. In panel (b), the doublet of peaks near 750 cm^{-1} is missing, while in panel (c), the intensities in the (0,*n*,0) progression are not well reproduced, while other peaks above 1700 cm^{-1} are either missing or given too much intensity.

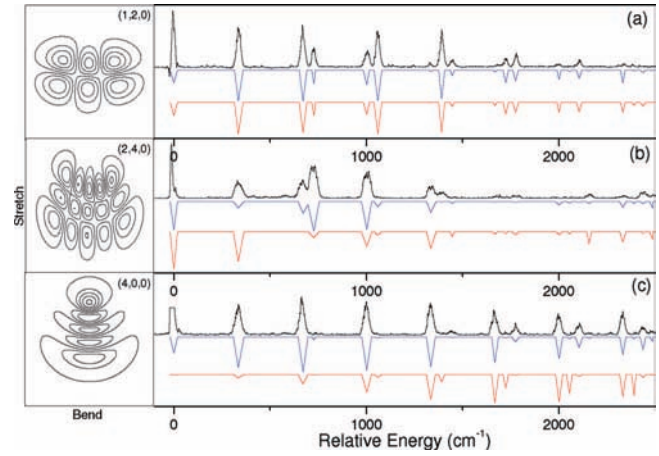

Figure 2. Experimental single vibronic level SVL emission spectra (top of each panel), compared with predicted intensities based on Model 1 (bottom spectrum in each panel) and the fit results of our polyad model (middle). Panel (a) is a level in $p = 4$, and the other two are from $p = 8$. On the left are the calculated wave functions for the emitting state, with a zeroth-order label corresponding to the highest contributing state within the polyad.

The intensities of transitions in a SVL fluorescence spectrum are very sensitive to the zeroth-order composition of the emitting state. To account for this, we conducted an analysis of the SVL fluorescence spectra based on Model 2. We analyzed spectra from over 36 excited-state levels between 18 100 and 20 700 cm^{-1} ($p = 3-11$), which included levels with and without significant mixing. To simulate the spectra we initially used harmonic Franck−Condon (FC) factors determined previously[41] and the well-known ground-state vibrational term energies. Each transition intensity was weighted by ν^3, based upon the frequency dependence of the Einstein (A) coefficient for spontaneous emission, and scaled for the response of the PMT, as provided by the manufacturer.

The intensity for a simulated emission transition, $I_{i,l}$, from eigenstate i to lower state l, was represented as

$$I_{i,l} = \left(\sum_j c_{ij} \mathrm{FCF}_{jl} \right)^2 \nu_{il}^{\ 3} \Gamma(\lambda) \tag{5}$$

where υ_{il} is the transition frequency, and FCF_{jl} is the FC factor for emission from zeroth-order state $|j\rangle$ to ground state $|l\rangle$. It is assumed that the ground-state levels are not mixed.[22,41] $\Gamma(\lambda)$ is the PMT correction, and c_{ij} are the mixing coefficients from eq 3. The sum over j runs over all zeroth-order states in a given polyad. The final intensity of each peak in an SVL fluorescence spectrum is very sensitive to the mixing coefficients; significant

transition moment interference can occur when the terms in the expansion, $c_{ij} \times FCF_{jl}$, are of opposite sign (both c_{ij} and FCF_{ij} can be positive or negative).

First, we performed unconstrained fits to the experimental intensities, allowing the c_{ij} to vary to optimize the fit. Fitting in this way allows the experimental spectrum to decompose itself into zero-order components without resorting to a particular model. The c_{ij} can be simply normalized for each mixed state $|i\rangle$. Ideally, the c_{ij} matrix would also be normalized for each zero-order component, i.e., the c_{ij} matrix is Hermitian. However, in practice, small changes in the experimental intensities cause the coefficient matrix to be non-Hermitian. We therefore compared the coefficients to those calculated from Model 2, where the Fermi resonance term $k_{122} = -4.2$ cm^{-1}. While the unconstrained fit obviously had a smaller error between experimental and simulated intensities, the predicted composition of the states (from Model 2) was not significantly different and the predicted intensities were in satisfactory agreement (χ^2 within a factor of 2 of the unconstrained fit).

The results of our fitting using $k_{122} = -4.2$ cm^{-1} are also shown in Figure 2a−c as the upper simulation in each panel. There is little difference between the "pure" and mixed simulation for $p = 4$, with both reproducing the experimental intensities well. In panel (b), we see both peaks around 750 cm^{-1} predicted, and peak intensities are well matched for the stronger peaks in the spectrum. The strong v_2 FC envelope in panel (c), peaking at $v = 2$, matches the experimental spectrum very well, and the simulation correctly predicts the intensities for the peaks above 1700 cm^{-1}. Overall, the simulation of experimental intensities is greatly improved when mixing within a polyad is accounted for.

We next determined mixing coefficients for a range of k_{122} values and used these to generate simulated emission intensities. Larger values of k_{122} predicted too strong a degree of mixing between states, with the calculated intensities a much worse fit. Smaller values, down to $k_{122} = -3.0$ cm^{-1}, gave mixing coefficients that fit the experimental data as well as those for $k_{122} = -4.2$ cm^{-1}. A value of $k_{122} = -3.0$ cm^{-1} in the Model 2 calculations also provides a reasonable fit to the observed vibrational terms, with an average difference for the 35,35 isotopologue of 2.4 cm^{-1}. Therefore, the combination of SVL intensities and term energies (i.e., fitting eigenvalues and eigenvectors) provides $k_{122} = -3.6 \pm 0.6$ cm^{-1} for all polyads up to $p = 9$.

The wave functions for the three excited vibrational states in Figure 2 are shown alongside the respective SVL spectra. They were calculated using harmonic oscillator wave functions and weighted using the mixing coefficients determined from $k_{122} = -4.2$ cm^{-1}. The wave functions are plotted as bend against stretch, with the number of vertical nodal planes showing the number of quanta of bend, and the horizontal planes the number of quanta of symmetric stretch. The $p = 4$ wave function is readily identifiable as (1,2,0), with two nodes along the bending coordinate and one mode along the stretching coordinate. The wave functions for the two $p = 8$ levels, while still identifiable as (2,4,0) and (4,0,0), show the effects of mixing as the nodes no longer lie directly along the bending and stretching coordinates. Secondary nodes can also be observed in both wave functions, with the central antinode (in the bending coordinate for the wave function labeled (2,4,0), and the stretching coordinate for the wave function labeled (4,0,0)) too strong for harmonic oscillator wave functions, where the main intensity would be expected at the extremities of the wave function. This mixing in of intensity from other eigenstates again illustrates

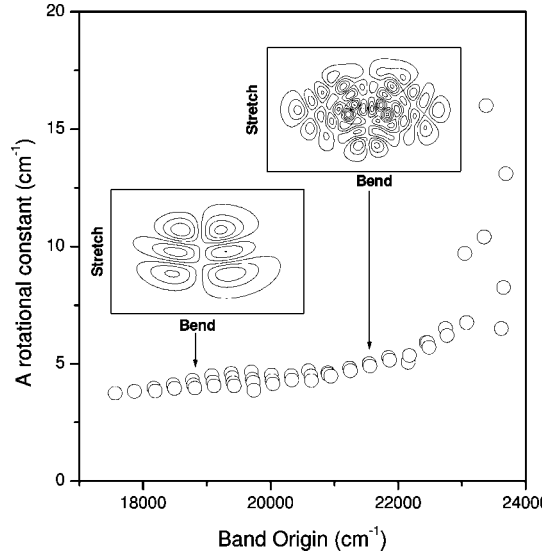

Figure 3. Measured A rotational constants for $C^{35}Cl_2$ bands obtained in this work plotted vs energy. A sudden increase near 23 000 cm^{-1} marks the approach to linearity and the RT intersection. Calculated wave functions are shown for two polyads, illustrating the degree of mixing at higher energies.

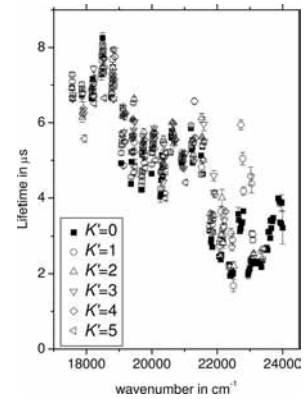

Figure 4. Fluorescence lifetimes measured in this work, sorted as a function of K'_a.

that the zeroth-order labels are no longer appropriate for the experimentally observed states.

The wave functions become increasingly mixed for higher polyads and zero-order labels become impossible to identify. An example of a wave function from the $p = 15$ polyad, calculated as above, is shown in the upper inset to Figure 3. This is in the part of the spectrum previously labeled as Region 2, in which assignment of the fluorescence excitation spectrum proved difficult. The wave function shows clearly that conventional assignment as bending and stretching quanta is inappropriate, and a simple polyad label is more useful to describe the states. SVL fluorescence spectra were also measured for most of the states throughout this region, and we attempted to fit the SVL spectra from this region as was done above; however, with so many zero-order states to include, and such highly oscillatory wave functions, there are many disparate local minima in the fit, and small changes in the experimental intensities can change the final fit significantly. Nonetheless, this analysis demonstrates clearly that the origin of the state mixing is anharmonic coupling. There is no real physical differentiation between Regions 1 and 2, which are only differentiated by the increasing number of states in the polyad and the size of the coefficients falling below that which allows a zero-order assignment of the peak.

D. Renner−Teller Intersection. Having successfully explained the vibrational mixing responsible for the transition from the previously labeled Region 1 to Region 2, we now turn to the Renner−Teller intersection. In related systems such as CHF where this intersection occurs at an energy stable with respect to dissociation, the approach to the RT intersection is evidenced in (i) a dramatic increase in the A rotational constant, and (ii) a loss of intensity for sub-bands terminating in $K'_a > 0$, with an associated increase in fluorescence lifetime.[26,27] The latter is due to mixing among vibrational levels of the RT pair of states, which scales with K_a^2 and is maximal in the barrier region where the wave functions strongly overlap. The energy dependence of the A rotational constant for CCl_2 is shown in Figure 3. For related systems such as CBr_2,[81] this energy dependence is found to be linear with vibrational quanta, and can be expressed as[82]

$$A(v_1, v_2) = A_{00} - \alpha_1 v_1 - \alpha_2 v_2 \quad (6)$$

where the α_i are the vibration−rotation interaction parameters, conventionally defined.[80,82] In order to model the dependence for CCl_2, we used eq 6 and effective quantum numbers generated using the mixing coefficients from Model 2 for $k_{122} = -4.2$ cm^{-1}. This approach gave a reasonable fit ($\sigma = 0.01$ cm^{-1}) up to 20 000 cm^{-1}, where the mixing becomes severe. The derived fit parameters are (in cm^{-1}): $A_{00} = 3.60(3)$, $\alpha_1 = -0.07(1)$, $\alpha_2 = -0.14(1)$.

Figure 3 has two interesting features. First, a coalescence of the A values can be observed from ∼20 900 cm^{-1} and above, due to the strong mixing between states at these energies which was discussed in sections A and C. The wave functions for two states (from $p = 5$ and $p = 15$) are shown, illustrating how strongly mixed the higher levels are. Second, one can note from Figure 3 the relatively smooth increase of A with energy up to ∼23 000 cm^{-1}, where an abrupt increase is observed. We attribute this increase to the approach to linearity and the RT intersection, a hypothesis which was tested using fluorescence lifetime measurements.

Figure 4 displays a compilation of the fluorescence lifetimes measured in this work, which are sorted as a function of K'_a. The lifetimes were measured by exciting sharp, isolated ^rR_K bandheads, and thus are averaged over several J levels. Where the uncertainties are not visible, they are smaller than the symbol size. Note that these results are not further sorted by isotopologue, as we found to within our uncertainty no dependence of the lifetime on isotopologue $C^{35}Cl_2$ vs $C^{35}Cl^{37}Cl$.

Our lifetimes are in mixed agreement with previous work. In early matrix studies, Bondybey reported a lifetime of 3.6 μs in solid Ar.[36] Because of fast vibrational relaxation in the matrix, this represents the value for the origin of the $\tilde{X} \rightarrow \tilde{A}$ system, which was not measured in this work due to a small intensity. For a related carbene, CF_2, where both matrix and gas-phase lifetimes are known,[83,84] the Ar matrix lifetime is ∼2.4 times shorter than that observed in the gas-phase. Applying this matrix correction to the Bondybey value gives a gas-phase lifetime of ∼8.5 μs, in good agreement with our results (Figure 4). Later, in room-temperature cell experiments, Thrush and co-workers reported values of 3.81(30) and 4.55(68) μs following excitation at 445−517 and 437 nm, respectively.[38] This trend is opposite that expected based on the wavelength dependence of the Einstein A coefficient, but in hindsight is understandable given the lifetime lengthening we observe at higher energy, described below. In another study, Shobotake and co-workers observed the $\tilde{A} \rightarrow \tilde{X}$ emission following VUV excitation of halogenated methanes, and reported biexponential decays with lifetimes near 2 and 4 μs, respectively.[57] We find no evidence for biexponential decays following the excitation of single vibronic levels, and our measured $K'_a = 0$ lifetimes gradually decrease from ∼7 μs at lower energy to ∼2 μs in the high-energy region of the spectrum.

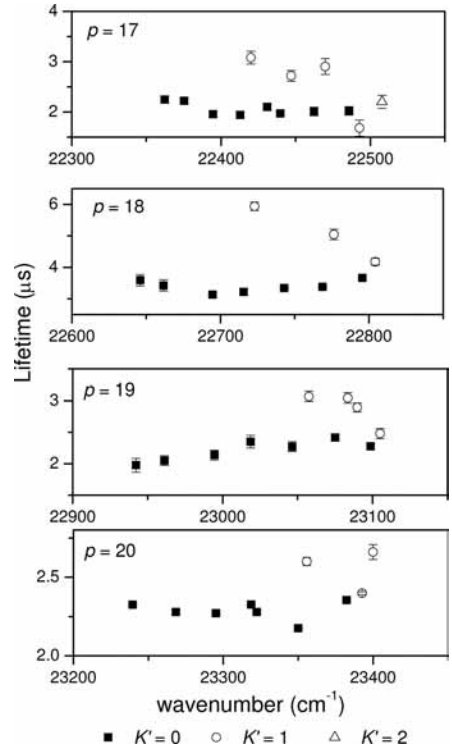

Figure 5. Expanded view of the lifetime data of polyads ($p = 17-20$) near the RT intersection. A pronounced lifetime lengthening for levels with $K'_a > 0$ is observed, so that very few lifetimes for these levels could be measured.

It is obvious from Figure 4 that there is little dependence of the lifetime on K'_a over much of the measured range. However, beginning at ∼22 500 cm^{-1}, a significant lengthening in lifetime is observed for levels with $K'_a > 0$, so that above ∼23 500 cm^{-1} only lifetimes for sub-bands terminating in $K'_a = 0$ could be measured, due to the extreme weakness of sub-bands with $K'_a > 0$. The transition to this region is illustrated in Figure 5, which displays expanded views of the lifetime measurements for four polyads ($p = 17-20$). Very few lifetimes could be measured for levels with $K'_a > 0$, and most of these have $K'_a = 1$. This is expected based on the K_a^2 scaling of the RT interaction and is consistent with simulations of spectra in this region, which show a severe weakening and eventual disappearance of sub-bands with $K'_a > 0$.[41] We emphasize that the weakening of these sub-bands reflects the spreading out of oscillator strength over many states. Taken with the energy dependence of the A rotational constant (Figure 3), the lifetime measurements indicate that the RT intersection occurs between 23 000 and 23 500 cm^{-1} above the vibrationless level of the $\tilde{X}^1A_1$ state, in close agreement with the theoretical (CASPT2[g1]/cc-pVTZ) prediction of 23 323 cm^{-1} by Sendt and Bacskay.[68]

IV. Conclusions

In an effort to unravel the complicated structure of the CCl_2 $\tilde{A}^1B_1 \leftarrow \tilde{X}^1A_1$ system, we have remeasured the spectrum from ∼17 500 to 24 000 cm^{-1}, or from polyad $p = 1$ to $p = 21$, and report the term energies and A rotational constants of many new bands for both major isotopologues ($C^{35}Cl_2$, $C^{35}Cl^{37}Cl$). We

fitted the observed term energies to a polyad effective Hamiltonian model and have demonstrated that a single resonance term accounts for most of the observed mixing. The vibrational parameters derived from this model are in excellent agreement with ab initio predictions, and the mixing coefficients deduced from the polyad model fit are in close agreement with those derived from direct fits of single vibronic level (SVL) emission intensities. We examined the approach to the barrier to linearity (RT intersection) through the energy dependence of the *A* rotational constant and fluorescence lifetime measurements, which indicate a barrier height that is in excellent agreement with ab initio theory.

Acknowledgment. S.A.R. gratefully acknowledges the National Science Foundation (grants CHE-0717960 and CHE-0353596) for support of this research. The research at Sydney was supported by the Australian Research Council (grant DP0347150). We acknowledge Dr. Joseph Guss for participating in early experiments on this work, and S.A.R. acknowledges valuable discussions with Prof. William Polik and Mr. Christopher Jordan of Hope College.

Supporting Information Available: Tables S1 and S2 of the wave functions for $C^{35}Cl_2$ and $C^{35}Cl^{37}Cl$ derived from our polyad analysis, and Figure S1 of experimental and simulated spectra for all of the polyads measured in this work. This information is available free of charge via the Internet at http://pubs.acs.org.

References and Notes

(1) *Carbenes*; Moss, R. A., Jones Jr., M., Eds.; Vol. I−II in Reactive Intermediates in Organic Chemistry Series; Wiley-Interscience: New York, 1973 (Vol. I); 1975 (Vol. II).
(2) Kirmse, W. *Carbene Chemistry*, 2nd ed.; Academic:New York, 1971.
(3) Sciano, J. C. In *Handbook of Organic Photochemistry*; CRC Press: Boca Raton, FL, 1989; Vol. 2, Chapter 9.
(4) Carey, F. A.; Sundberg, R. J. In *Advanced Organic Chemistry*; Part 3, 3rd ed.; Plenum: New York, 1990.
(5) Weirsum, U. E.; Jenneskens, L. W. In *Gas Phase Reactions in Organic Synthesis*; Vallée, Y., Ed.; Gordon and Breach: Amsterdam, The Netherlands, 1997.
(6) Dean, A. M.; Bozzelli, J. W. In *Gas-phase Combustion Chemistry*; Gardiner Jr., W. C., Ed.; Springer: New York, 2000; Chapter 2.
(7) Murray, K. K.; Leopold, D. G.; Miller, T. M.; Lineberger, W. C. *J. Chem. Phys.* **1988**, *89*, 5442.
(8) Tarczay, G.; Miller, T. A.; Czakó, G.; Császár, A. G. *Phys. Chem. Chem. Phys.* **2005**, *7*, 2881.
(9) Schwartz, R. L.; Davico, G. E.; Ramond, T. M.; Lineberger, W. C. *J. Phys. Chem. A* **1999**, *103*, 8213.
(10) Chen, C.-W.; Tsai, T.-C.; Chang, B.-C. *Chem. Phys. Lett.* **2001**, *347*, 73.
(11) Chen, C.-W.; Tsai, T.-C.; Chang, B.-C. *J. Mol. Spectrosc.* **2001**, *209*, 254.
(12) Tsai, T.-C.; Chen, C.-W.; Chang, B.-C. *J. Chem. Phys.* **2001**, *115*, 766.
(13) Yu, H.-G.; Lezana-Gonzalez, T.; Marr, A. J.; Muckerman, J. T.; Sears, T. J. *J. Chem. Phys.* **2001**, *115*, 5433.
(14) Lee, C.-L.; Liu, M.-L.; Chang, B.-C. *J. Chem. Phys.* **2002**, *117*, 3263.
(15) Lee, C.-L.; Liu, M.-L.; Chang, B.-C. *Phys. Chem. Chem. Phys.* **2003**, *5*, 3859.
(16) Liu, M.-L.; Lee, C.-L.; Bezant, A.; Tarczay, G.; Clark, R. J.; Miller, T. A.; Chang, B.-C. *Phys. Chem. Chem. Phys.* **2003**, *5*, 1352.
(17) Lin, C.-S.; Chen, Y.-E.; Chang, B.-C. *J. Chem. Phys.* **2004**, *121*, 4164.
(18) Chang, W.-Z.; Hsu, H.-J.; Chang, B.-C. *Chem. Phys. Lett.* **2005**, *413*, 25.
(19) Gilles, M. K.; Ervin, K. M.; Ho, J.; Lineberger, W. C. *J. Phys. Chem.* **1992**, *96*, 1130.
(20) Deselnicu, M.; Mukarakate, C.; Tao, C.; Reid, S. A. *J. Chem. Phys.* **2006**, *124*, 134302.
(21) Tao, C.; Mukarakate, C.; Reid, S. A. *J. Chem. Phys.* **2006**, *124*, 224314.
(22) Mukarakate, C.; Mishchenko, Y.; Brusse, D.; Tao, C.; Reid, S. A. *Phys. Chem. Chem. Phys.* **2006**, *8*, 4320.
(23) Tao, C.; Mukarakate, C.; Judge, R. H.; Reid, S. A. *J. Chem. Phys.* **2008**, *128*, 171101.
(24) Knepp, P. T.; Kable, S. H. *J. Chem. Phys.* **1999**, *110*, 11789.
(25) Guss, J. S.; Votava, O.; Kable, S. H. *J. Chem. Phys.* **2001**, *115*, 11118.
(26) Fan, H.; Ionescu, I.; Annesley, C.; Reid, S. A. *Chem. Phys. Lett.* **2003**, *378*, 548.
(27) Fan, H.; Ionescu, I.; Annesley, C.; Cummins, J.; Bowers, M.; Xin, J.; Reid, S. A. *J. Phys. Chem. A* **2004**, *108*, 3732.
(28) Schmidt, T. W.; Bacskay, G. B.; Kable, S. H. *J. Chem. Phys.* **1999**, *110*, 11277.
(29) Schmidt, T. W.; Bacskay, G. B.; Kable, S. H. *Chem. Phys. Lett.* **1998**, *292*, 80.
(30) Ionescu, I.; Fan, H.; Annesley, C.; Xin, J.; Reid, S. A. *J. Chem. Phys.* **2004**, *120*, 1164.
(31) Fan, H.; Ionescu, I.; Xin, J.; Reid, S. A. *J. Chem. Phys.* **2004**, *121*, 8869.
(32) Ionescu, I.; Fan, H.; Ionescu, E.; Reid, S. A. *J. Chem. Phys.* **2004**, *121*, 8874.
(33) Milligan, D. E.; Jacox, M. E. *J. Chem. Phys.* **1967**, *47*, 703.
(34) Shirk, J. S. *J. Chem. Phys.* **1971**, *55*, 3608.
(35) Tevault, D. E.; Andrews, L. *J. Mol. Spectrosc.* **1975**, *54*, 110.
(36) Bondybey, V. E. *J. Mol. Spectrosc.* **1977**, *64*, 180.
(37) Bauschlicher, Jr., C. W.; Schaefer III, H. F.; Bagus, P. S. *J. Am. Chem. Soc.* **1977**, *99*, 7106.
(38) Huie, R. E.; Long, N. J. T.; Thrush, B. A. *Chem. Phys. Lett.* **1977**, *51*, 197.
(39) Ha, T.-K.; Gremlich, H. U.; Buehler, R. E. *Chem. Phys. Lett.* **1979**, *65*, 16.
(40) Tiee, J. J.; Wampler, F. B.; Rice, W. W. *Chem. Phys. Lett.* **1979**, *65*, 425.
(41) Guss, J. S.; Richmond, C. A.; Nauta, K.; Kable, S. H. *Phys. Chem. Chem. Phys.* **2005**, *7*, 100.
(42) Clouthier, D. J.; Karolczak, J. *J. Phys. Chem.* **1989**, *93*, 7542.
(43) Clouthier, D. J.; Karolczak, J. *J. Chem. Phys.* **1991**, *94*, 1.
(44) Schlacta, R.; Lack, G.; Tsay, S. H.; Bondybey, V. E. *Chem. Phys.* **1991**, *155*, 267.
(45) Xu, S.; Harmony, M. D. *Chem. Phys. Lett.* **1993**, *205*, 502.
(46) Carter, E. A.; Goddard III, W. A. *J. Chem. Phys.* **1988**, *88*, 1752.
(47) Nguyen, M. T.; Kerins, M. C.; Hegarty, A. F.; Fitzpatrick, N. J. *Chem. Phys. Lett.* **1985**, *117*, 295.
(48) Choe, J. I.; Tanner, S. R.; Harmony, M. D. *J. Mol. Spectrosc.* **1989**, *138*, 319.
(49) Shin, S. K.; Goddard III, W. A.; Beauchamp, J. L. *J. Phys. Chem.* **1990**, *94*, 6963.
(50) Ibuki, T.; Takahashi, N.; Hiraya, A.; Shobatake, K. *J. Chem. Phys.* **1986**, *85*, 5717.
(51) Kim, S. J.; Hamilton, T. P.; Schaefer III, H. F. *J. Chem. Phys.* **1991**, *94*, 2063.
(52) Li, Q.; Chen, Y.; Wang, D.; Zhang, Y.; Yu, S.; Chen, C.; Koshi, M.; Matsui, H.; Koda, S.; Ma, X. *Chem. Phys. Lett.* **1991**, *178*, 517.
(53) Paulino, J. A.; Squires, R. R. *J. Am. Chem. Soc.* **1991**, *113*, 5573.
(54) Gutsev, G. L.; Ziegler, T. *J. Phys. Chem.* **1991**, *95*, 7220.
(55) Lee, L. C.; Suto, M. *Chem. Phys.* **1987**, *114*, 423.
(56) Irikura, K. K.; Goddard III, W. A.; Beauchamp, J. L. *J. Am. Chem. Soc.* **1992**, *114*, 48.
(57) Ibuki, T.; Atsunari, H.; Shobatake, K. *J. Chem. Phys.* **1992**, *96*, 8793.
(58) Russo, N.; Sicilia, E.; Toscano, M. *J. Chem. Phys.* **1992**, *97*, 5031.
(59) Carter, E. A.; Goddard III, W. A. *J. Phys. Chem.* **1987**, *91*, 4651.
(60) Cai, Z.-L.; Zhang, X.-G.; Wang, X.-Y. *Chem. Phys. Lett.* **1993**, *210*, 481.
(61) Gobbi, A.; Frenking, G. *J. Chem. Soc., Chem. Commun.* **1993**, *14*, 1162.
(62) Morley, G. P.; Felder, P.; Huber, J. R. *Chem. Phys. Lett.* **1994**, *219*, 195.
(63) Garcia, V. M.; Castell, O.; Reguero, M.; Callol, R. *Mol. Phys.* **1996**, *87*, 1395.
(64) Cheong, B.-S.; Cho, H.-G. *J. Phys. Chem. A* **1997**, *101*, 7901.
(65) Kumaran, S. S.; Su, M.-C.; Lim, K. P.; Michael, J. V.; Klippenstein, S. J.; DiFelice, J.; Mudipalli, P. S.; Kiefer, J. H.; Dixon, D. A.; Peterson, K. A. *J. Phys. Chem. A* **1997**, *101*, 8653.
(66) Das, D.; Whittenburg, S. L. *J. Mol. Structure: THEOCHEM* **1999**, *492*, 175.
(67) Schwartz, M.; Marshall, P. *J. Phys. Chem. A* **1999**, *103*, 7900.
(68) Sendt, K.; Bacskay, G. B. *J. Chem. Phys.* **2000**, *112*, 2227.
(69) Barden, C. J.; Schaefer III, H. F. *J. Chem. Phys.* **2000**, *112*, 6515.
(70) Lee, E. P. F.; Dyke, J. M.; Wright, T. G. *Chem. Phys. Lett.* **2000**, *326*, 143.
(71) Hansen, N.; Mader, H.; Temps, F. *Phys. Chem. Chem. Phys.* **2001**, *3*, 50.

(72) Dixon, D. A.; Peterson, K. A. *J. Chem. Phys.* **2001**, *115*, 6327.
(73) Gao, Y.; Ran, Q.; Chen, Y.; Chen, C. *Int. J. Chem. Kinet.* **2002**, *34*, 351.
(74) Mueller, P. H.; Rondan, N. G.; Houk, K. N.; Harrison, J. F.; Hooper, D.; Willen, B. H.; Liebman, J. F. *J. Am. Chem. Soc.* **1981**, *103*, 5049.
(75) Chu, G.; Moss, R. A.; Sauers, R. R. *J. Am. Chem. Soc.* **2005**, *127*, 14206.
(76) McKee, M. L.; Michl, J. *J. Phys. Chem. A* **2002**, *106*, 8495.
(77) Dyke, J. M.; Lee, E. P. F.; Mok, D. K. W.; Chau, F.-T. *ChemPhysChem* **2005**, *6*, 2046.
(78) Shin, S. K.; Dagdigian, P. J. *J. Chem. Phys.* **2006**, *125*, 133317.
(79) Shin, S. K.; Dagdigian, P. J. *Phys. Chem. Chem. Phys.* **2006**, *8*, 3446.
(80) Herzberg, G. *Molecular Spectra and Molecular Structure II. Infrared and Raman Spectra of of Polyatomic Molecules*; Van Nostrand: New York, 1945; pp 205−208.
(81) Tao, C.; Mukarakate, C.; Brusse, D.; Mishchenko, Y.; Reid, S. A. *J. Mol. Spectrosc.* **2007**, *241*, 180.
(82) Nielsen, H. H. *Rev. Mod. Phys.* **1951**, *23*, 90.
(83) Cameron, M. R.; Kable, S. H. *J. Mol. Spectrosc.* **1998**, *192*, 449.
(84) Bondybey, V. E. *J. Mol. Spectrosc.* **1976**, *63*, 164.

JP806944Q